Published in final edited form as:
J Orthop Res. 2009 January ; 27(1): 71–77. doi:10.1002/jor.20702.

The Association Between Velocity of the Center of Closest Proximity on Subchondral Bones and Osteoarthritis Progression

William J. Anderst and **Scott Tashman**
Department of Orthopaedics, University of Pittsburgh, Pittsburgh, PA

Abstract

Altered surface interactions following joint instability may apply novel, damaging loads to articular cartilage. This study measured the velocity of the centers of closest proximity on subchondral bone surfaces on the femur and tibia during running in normal and unstable canine stifle (knee) joints. The purpose was to explore the relationship between the velocity of the centers of closest proximity on subchondral bones and the severity of cartilage damage. Dynamic biplane radiography was used to acquire serial knee kinematics (5 control, 18 CCL-deficient) during treadmill running over two years. Custom software calculated the difference between the rate at which the center of closest proximity on the femur translated relative to the femur bone surface and the rate at which the center of closest proximity on the tibia translated relative to the tibia bone surface. Comparisons were made between dogs that developed minor versus major medial compartment cartilage damage over two years. Major damage dogs showed a significantly greater increase in the difference between femur and tibia medial compartment closest proximity point velocity from the instant of paw strike to peak velocity difference at 2, 4 and 6 months after CCL-transaction. This implies increased tangential forces associated with the velocity of the compressed cartilage region during joint movement (plowing) may be a mechanism that initiates OA development and drives OA progression. In the future, articulating surface velocity measurements may be useful to identify patients at risk for long term OA due to joint instability.

Keywords

velocity; mechanical factors; canine; knee; plowing

Introduction

Joint instability may lead to modified and excessive mechanical stresses on the articular surfaces. This repetitive, chronic mechanical overload is one possible source behind the initiation and progression of osteoarthritis. However, the mechanisms by which excessive mechanical force may lead to OA remain unknown.

It has been proposed that knee OA has an initiation phase and a progression phase1. The initiation phase is characterized by a change in the location of load bearing regions following joint instability. Researchers have suggested that loading regions of articular cartilage not accustomed to load may lead to OA2,3. Theoretical models4,5 have predicted changes in load bearing region location within unstable joints, while *in vivo* static measurements have indicated a difference in cartilage contact location between intact and ACL-deficient knees6,7.

Corresponding Author: William Anderst, Biodynamics Lab, Department of Orthopaedic Surgery, 3820 South Water Street, Pittsburgh, PA 15203, Tel: 412-586-3946, Fax: 412-586-3979, email: anderst@pitt.edu.

The progression phase of OA is purportedly driven by increased tangential shear loading1. The increased shear loading may be due to an increased coefficient of friction between articulating surfaces associated with surface fibrillation. This fibrillation may develop following excessive loading of the tissues. The excessive loading may occur due to a change in the load bearing regions, as has been previously proposed1.

In addition to altered contact locations, modifications in sliding, rolling and pivoting contacts may impart unaccustomed and excessive load to the articular surfaces. In particular, increasing contact velocity may increase the plowing forces applied to the articular cartilage, as has been demonstrated using various materials and lubricants to investigate articular cartilage mechanics8¯11. Plowing friction results from the incremental sequential compression deformation of the cartilage accompanying joint motion12،13. The current research investigates this additional mechanism for the initiation and progression of OA--the way in which the articulating surfaces interact may be related to the severity of long-term articular cartilage damage.

Our group has previously published detailed kinematic measurements obtained from the subjects in this study14. Traditional kinematic measurements (joint translations and rotations) revealed abnormal anterior translation and abduction in cranial cruciate ligament (CCL)-transected dogs14. Further analysis led to the observation that there was a range of articular cartilage damage among the subjects, just as there is variation in the progression of OA following ACL loss in humans15. The observed variability in articular cartilage damage provided motivation for further study to attempt to identify mechanical factors that were associated with the long-term severity of OA. If mechanical factors associated with long-term severe OA can be identified soon after joint instability develops, perhaps steps can be taken to impede the progression of OA (e.g. surgery, muscle strengthening, etc.). The current study was performed to attempt to identify *in vivo* mechanical factors that may be associated with OA development and progression.

The current study measured the velocity of the points in closest proximity on the subchondral surfaces of the femur and tibia during running in stable and unstable canine stifle (knee) joints. The goals of the study were to characterize the interaction between the tibia and femur centers of closest proximity in the uninjured joint during running (e.g. rolling versus sliding contacts), to discover how these interactions changed in the unstable joint, and to determine if there was an association between subchondral closest proximity point velocity and the severity of cartilage damage in the unstable joints. It was hypothesized that intact joints would display a combination of sliding and rolling contact, joint instability would significantly alter proximal subchondral point velocity on each subchondral surface, and the severity of articular cartilage degeneration would be related to the velocity of the proximal subchondral point in unstable joints.

Methods

After approval from our Institutional Animal Care and Use Committee, 23 skeletally mature female foxhounds served as subjects. At least three 1.6 mm diameter tantalum beads were implanted into both the right distal femur and right proximal tibia at the initiation of the study. Testing consisted of running on a treadmill set at 1.5 m/s. During treadmill running, dogs were x-rayed using a biplane radiographic imaging system capable of tracking the implanted beads with an accuracy of better than ± 0.10 mm16. All dogs underwent a second surgery after the first test session. Eighteen dogs received a complete transection of the cranial cruciate ligament (CCL) (analogous to the ACL in humans), while five dogs underwent a sham operation in which the CCL was exposed but not cut. Dogs received regular exercise throughout the study (30 min of treadmill running three times per week).

Dogs were tested running on the treadmill nine more times after the second surgery (2, 4, 6, 8, 10, 12, 16, 20 and 24 months post-surgery).

X-ray images were collected at 250 frames per second from 200 ms prior to paw strike to 400 ms after paw strike. Implanted beads were identified in each radiographic image using custom software, and two-dimensional bead coordinates were input to a commercial software package (Eva, Motion Analysis Corp., Santa Rosa, CA) for tracking and three-dimensional (3D) reconstruction.

Computed tomography (CT) data of the femur and tibia were collected after sacrifice and reconstructed into 3D wireframe meshes consisting of triangular elements17. The 3D location of each implanted bead was identified within each CT scan reconstruction. Implanted bead locations from CT scans were combined with 3D bead coordinates acquired during treadmill running to precisely position the femur and tibia CT reconstructions for each frame of treadmill running. The minimum distance between articulating subchondral bone surfaces was determined at each surface triangle for each bone for each frame of data18. Bone surface triangles were grouped into four regions of interest (ROIs) (medial, lateral femur; medial, lateral tibia). Surface triangles within femur ROIs were expressed in cylindrical coordinate systems (with the long axis of the cylinder defined by a line from the medial to lateral condyle and the arc of the cylinder following the curve of the femur condyle in the sagittal plane), while surface triangles within tibia ROIs were expressed in orthogonal coordinate systems (with a medial-lateral axis, anterior-posterior and proximal-distal axis as described previously13, with the ROI rotated about the sagittal axis such that the plane defined by the medial/lateral and anterior/posterior axes was parallel to the tibia articulating surface). The weighted centroid on the bone surface reconstruction was determined by each triangle's area and distance to the opposing surface for each ROI, similar to the technique described in detail previously18. This point, called the proximal subchondral point (PSP), defined the center of closest proximity on the subchondral bone surface. The location of the PSP in each ROI was determined for each frame of the loading phase (paw strike to 200 ms after paw strike). These location values were differentiated using a four point weighted least-squares approach19 to determine velocity of each PSP within it's respective ROI coordinate system. It should be noted that these proximal subchondral points were located on the subchondral bone surfaces, not the articular cartilage surfaces. Their velocity will be referred to as “proximal subchondral point velocity,” abbreviated PSP_v for clarity, throughout the remainder of this manuscript. The PSP_v reflects the velocity at which the calculated proximal subchondral point traveled on the bone surface relative to each ROI described above.

PSP_v components tangent to the femur subchondral surfaces were calculated using the formula $vTANGENT = \sqrt{\left(\omega_o \times \frac{\pi}{180^\circ} \times r_2\right)^2 + v_1^2}$, where ω_o was the angular velocity of the PSP in the direction of the region of interest arc, r_2 was the distance from the long axis of the cylindrical coordinate system (the medial-lateral anatomical axis) to the PSP, and v_1 was the velocity of the PSP tangent to the subchondral surface and perpendicular to the direction of the region of interest arc. For the tibia, PSP_v tangent to the subchondral surfaces was calculated using the formula $vTANGENT = \sqrt{v_1^2 + v_2^2}$, where v_1 and v_2 were the velocities of the PSP in the plane of the tibia ROI parallel to the tibia subchondral surface. The difference between the femur and tibia PSP velocities, $v_{DIFFERENCE}$, was calculated by subtracting the tibia tangential PSP_v from the femur tangential PSP_v, with positive values assigned to velocity in the anterior (cranial) direction of each ROI. Thus, $v_{DIFFERENCE}$ was a combined measure of the rate at which each PSP was translating tangent to it's respective bone surface.

At sacrifice, femur and tibia articulating surfaces were stained with India ink to identify location, size and severity of cartilage damage. Photos of all articulating surfaces were viewed by an anatomist/veterinarian and graded on a zero to four scale according to cartilage damage, similar to that which has been used previously20 (0 = no damage; 1 = visible surface damage/fibrillation; 2 = small regions of thinned cartilage, no full thickness defects; 3 = large regions of thinned cartilage and/or small full thickness defects; 4 = large regions of full thickness cartilage loss). Dogs were grouped for statistical tests according to total medial compartment damage using the sum of medial femur score plus medial tibia score, for a maximum possible score of eight. The midpoint of maximum possible damage (4) served as the cutoff between minor and major articular cartilage damage groups.

Average PSP_v tangent to the surface of each ROI was determined for each of the three groups (control, minor damage, major damage) on each test date. Significant differences in PSP_v curves were identified using a two-sample Kolmogorov-Smirnov test ($p < 0.05$) to compare 20 ms segments of each curve. Kolmogorov-Smirnov compares cumulative distribution functions for two groups to detect differences in shapes and locations (SPSS V15). This test is more reliable than the Pearson r and ANOVA in detecting differences between curves of data21. Medial compartment PSP_v difference ($v_{DIFFERENCE}$, from above) at paw strike, peak $v_{DIFFERENCE}$, and the change in $v_{DIFFERENCE}$ between these two instants were compared among the three groups using repeated measures analysis of variance (ANOVA) with test day as the repeated measure. Significance level was set to $p < 0.05$ with the Bonferroni correction applied to post hoc comparisons.

Results

The controls dogs all had cartilage damage scores less than two (n = 5; mean score = 0.40 ± 0.55), the minor damage group had damage scores from two to four (n = 9; mean score = 3.22 ± 0.83), and the major damage group had damage scores from five to eight (n = 9; mean score = 6.22 ± 0.97).

The average PSP_v curve within each ROI was consistent over the ten test sessions for the control group (Figure 1). The average standard deviations (SD) over the entire test protocol for the control dogs (error bars in Figure 1) were 8.7 mm/s, 5.8 mm/s, 9.4 mm/s and 9.1 mm/s for the lateral femur, lateral tibia, medial femur and medial tibia, respectively.

PSP_v in the control group was significantly different between the lateral femur and tibia for the first 40 ms following paw strike, and again from 80 ms to 180 ms after paw strike (Figure 1A). Medial femur PSP_v and medial tibia PSP_v, on the other hand, were significantly different for the first 100 ms following paw strike and from 140 to 200 ms after paw strike (Figure 1B).

The velocity difference between the proximal subchondral points in the control group was positive and not significantly different between the medial and lateral compartments the first 40 ms after paw strike (Figure 2). The velocity difference was significantly higher on the medial side than on the lateral side from 40 ms to 140 ms after paw strike, which included the end of extension and beginning of flexion. The peaks of the velocity difference curves occurred at paw strike in both the medial and lateral compartments, and in general the curves showed small variations between maximum and minimum velocity difference in either compartment. Control group velocity difference curves were repeatable, with average standard deviations of 8.6 mm/s in both the lateral and medial compartments (error bars in Figure 2).

Following CCL-transection, significant differences between femur and tibia PSP velocities on both the medial and lateral side persisted throughout extension and well into the flexion

phase, up to 140 ms after paw strike (Figure 3A and Figure 3B). Lateral compartment PSP_v near the transition from extension to flexion did not exhibit equal or nearly equal velocity on the femur and tibia as in the CCL-intact condition. The combination of more negative (posterior) PSP velocity within each tibia compartment and extended duration of positive (anterior) PSP velocity on the femur changed both the magnitude and the shape of the velocity difference curves for the minor and major damage groups (Figure 4A and Figure 4B). Following CCL transection, the peaks in the velocity difference curves occurred near the initiation of flexion, not at paw strike as in the CCL-intact condition. Peak velocity difference occurred when the PSP_v was large and positive (anterior) on the femur and large and negative (posterior) on the tibia.

Following paw strike, there was a rapid increase in velocity difference between the proximal subchondral points in the medial compartment in the unstable joint, most notably in the major damage group. The increase in the PSP_v difference curve from paw strike to curve peak (circles in Figure 5) was significantly larger in the major damage group than in the minor damage group 2, 4 and 6 months after CCL transection (Figure 6). This variation in velocity difference curves between minor and major damage groups resulted from the following combination of velocity changes: 1) a smaller decrease in tibia PSP velocity at paw strike in the major damage group (compared to the minor damage group), resulting in a smaller velocity difference between the femur and tibia at paw strike; 2) an increase in anterior (more positive) velocity of the PSP on the femur and larger posterior (more negative) velocity of the PSP on the tibia near the initiation of flexion in the major damage group (compared to the minor damage group), resulting in a larger peak velocity difference between the femur and tibia proximal subchondral points just after flexion began.

Kinematic results implied the joint was more unloaded following CCL-transection, however, the flexion curves were not different between CCL-deficient groups (Figure 7).

Discussion

Measurements from the control dogs over ten test sessions spanning a two-year period showed low variability and suggest that the velocity curves are a good representation of the behavior of intact knee joints in this population. PSP_v curves in intact knee joints revealed the following: First, the PSP_v on the femur and tibia was positive (anterior) from paw strike to maximum extension. As expected, PSP_v was generally negative (posterior) on the femur and tibia during flexion; second, the PSP_v was generally larger in magnitude on the femur than the tibia, implying the tibia slid on the femur for the majority of early stance; third, on the lateral side, for about 25 ms, the PSP_v difference was near zero. This occurred as the knee transitioned from extension to flexion. Simultaneously, on the medial side there was positive PSP_v on the femur and negative velocity on the tibia. This suggests that while a slow rolling or pivoting was occurring in the lateral compartment, sliding was occurring in the medial compartment, with the PSP moving in the anterior direction on the medial femur and posterior direction on the medial tibia. These motions are consistent with previously reported external rotation of the tibia relative to the femur following foot strike in these subjects14. Additionally, the present results imply that the pivot for the external rotation occurred near the PSP between the lateral femur and lateral tibia; and fourth, the maximum velocity difference between proximal suchondral points occurred at paw strike, and velocity difference curves covered a small range of values.

The PSP_v on the femur and tibia following CCL transection indicated a rapid sliding motion occurred between the femur and tibia the first 140 ms after paw strike. The primarily positive PSP_v on the femur and primarily negative PSP_v on the tibia reveal a sliding of the femur backward on the tibia and a sliding of the tibia forward on the femur in both

compartments. Approximately 140 ms after paw strike, the rapid translation between the femur and tibia terminated, likely due to the restraints of intact tendons and ligaments.

ACL loss in humans (and CCL loss in canines) has been associated with an increase in anterior translation of the tibia relative to the femur14,22-25 and a modification in rotation of the tibia relative to the femur3,22,23,25. Figures 4A and 4B, when compared to Figure 2, provide additional information beyond joint kinematics regarding the interactions between articulating surfaces following CCL loss. The near-zero velocity difference between PSPs in the lateral compartment at the initiation of flexion in the intact joint no longer existed after CCL loss, indicating there was no rolling or pivot about the lateral compartment. Additionally, the velocity difference between the PSPs was up to 2.5 times larger following CCL transection in both the medial and lateral compartments. This peak velocity difference tangent to the subchondral bone surfaces occurred near the time of peak ground reaction force26.

The current *in vivo* dynamic loading results show subjects that developed severe medial compartment cartilage damage following joint instability displayed a significantly greater increase in the medial compartment PSP_v difference than subjects that developed minor cartilage damage (Figure 6). It is possible this modified the loading pattern beyond the tolerance of the articular cartilage, thus increasing the severity of OA. A mechanism that can explain theses results has been referred to as plowing9-13 in the literature. Plowing forces have been reported to be at least an order of magnitude greater than the classic frictional forces when analyzing compression area velocity in the temporomandibular joint (TMJ) disc9. Furthermore, studies have found that the coefficient of friction9,10, contact stress27, shear stress28 and the friction force28 increase with sliding velocity. These studies attribute the increase in tractional forces (the sum of classic friction and plowing forces) to plowing. Interestingly, this increase in tractional force with increasing velocity has been reported when instantaneous velocity and coefficient of friction were collected8-11 but not during constant velocity tests13,29. Therefore, it may be that the *increase* in the velocity of the PSP is the quantity that is most closely related to the plowing forces the cartilage experiences. This view supports the results of the current study, as it was the *increase* in velocity difference between PSPs following paw strike that was related to the severity of cartilage damage.

The results of this study provide quantitative data to support the theory that a change in the way articulating surfaces move relative to each other may initiate the breakdown of collagen, leading to increased fibrillation, increased friction between surfaces and increased tangential shear. The mechanism for this increased friction and shear is the increase in velocity difference between PSPs on each subchondral bone surface. This increased velocity gradient may increase shear stress and influence OA development and progression, as shear stress is one mechanical factor that may influence articular cartilage degeneration30-32. It is possible that subjects that were able to make the proper neuromuscular adaptation following joint instability minimized the altered surface interactions and were able to lessen long-term cartilage damage, akin to ACL-deficient subjects who display kinematics33 and neuromuscular function34 similar to ACL-intact controls. The results of this study suggest the techniques presented here can be applied shortly after instability develops to identify subjects most likely to develop severe OA. It may be possible to train these subjects to modify their loading patterns and minimize cartilage damage due to mechanical factors, specifically shear stresses35.

Several limitations apply to the present study. First, the results were obtained in a canine model of OA, and may not necessarily apply to the development and progression of OA in humans. Second, force plate data was not collected, and it is possible that the minor damage

group unloaded the CCL-deficient leg more than the major damage group. However, kinematic evidence for unloading was not apparent, as differences in flexion/extension curves were not observed (Figure 7). Third, PSP location was determined on subchondral bone surfaces obtained from CT. Including soft tissue such as the meniscus and articular cartilage in the proximal point calculations may have altered the proximal point locations36. However, canine femur and tibia articular cartilage is less than 2 mm in combined thickness37, and the effect of including articular cartilage would have likely been minimal. In addition, meniscal deterioration was not quantified serially throughout the study, and the sequencing between meniscus failure, cartilage damage and increased velocity difference between subchondral surfaces is unknown. It is likely that modified surface interactions, such as the increased velocity difference reported here, subjected the articular cartilage and meniscus to forces beyond those to which they were accustomed, leading to cartilage damage, meniscal destruction and OA. Finally, the CT scan data was collected only at the end of the study, and changes in bone morphology may have occurred over the duration of the study.

The present analysis and previously published results of the dynamic joint space between the femur and tibia38 both presented variables to help identify subjects that developed long-term major and minor articular surface damage. While dynamic joint space measurements reveal thickness and mechanical properties of cartilage during functional loading, they do not provide a mechanical explanation for cartilage degradation. PSP_v differences, on the other hand, provide a mechanical mechanism that may drive OA development and progression. In addition, these techniques are site-specific, which may make them more effective in identifying adaptations and degeneration observed in osteoarthritic joints, which are also typically site-specific39,40.

Measurements related to articular surface mechanics may provide useful information regarding the need for surgical or rehabilitative interventions intended to prevent or slow the progression of osteoarthritis due to mechanical factors. In the future, these methods will be applied to investigate the relationship between compartment-specific articular surface interactions and OA development in human knees during dynamic *in vivo* loading.

Acknowledgments

National Institutes of Health Grant AR43860 funded this study. The authors thank Clifford M. Les, PhD, DVM for providing cartilage damage scores used in this study.

References

1. Andriacchi TP, Mundermann A, Smith RL, et al. A framework for the in vivo pathomechanics of osteoarthritis at the knee. Ann Biomed Eng. 2004; 32:447–457. [PubMed: 15095819]
2. Brandsson S, Karlsson J, Eriksson BI, et al. Kinematics after tear in the anterior cruciate ligament: Dynamic bilateral radiostereometric studies in 11 patients. Acta Orthop Scand. 2001; 72:372–378. [PubMed: 11580126]
3. Andriacchi TP, Dyrby CO. Interactions between kinematics and loading during walking for the normal and acl deficient knee. J Biomech. 2005; 38:293–298. [PubMed: 15598456]
4. Wu JZ, Herzog W, Epstein M. Joint contact mechanics in the early stages of osteoarthritis. Med Eng Phys. 2000; 22:1–12. [PubMed: 10817944]
5. Andriacchi TP, Briant PL, Bevill SL, et al. Rotational changes at the knee after acl injury cause cartilage thinning. Clin Orthop Relat Res. 2006; 442:39–44. [PubMed: 16394737]
6. Shefelbine SJ, Ma CB, Lee KY, et al. Mri analysis of in vivo meniscal and tibiofemoral kinematics in acl-deficient and normal knees. J Orthop Res. 2006; 24:1208–1217. [PubMed: 16652339]

7. Li G, Moses JM, Papannagari R, et al. Anterior cruciate ligament deficiency alters the in vivo motion of the tibiofemoral cartilage contact points in both the anteroposterior and mediolateral directions. J Bone Joint Surg Am. 2006; 88:1826–1834. [PubMed: 16882908]
8. Linn FC. Lubrication of animal joints. Ii. The mechanism. J Biomech. 1968; 1:193–205. [PubMed: 16329290]
9. Nickel JC, Iwasaki LR, Beatty MW, et al. Laboratory stresses and tractional forces on the tmj disc surface. J Dent Res. 2004; 83:650–654. [PubMed: 15271976]
10. Nickel JC, Iwasaki LR, Beatty MW, et al. Static and dynamic loading effects on temporomandibular joint disc tractional forces. J Dent Res. 2006; 85:809–813. [PubMed: 16931862]
11. Williams PF 3rd, Powell GL, LaBerge M. Sliding friction analysis of phosphatidylcholine as a boundary lubricant for articular cartilage. Proc Inst Mech Eng [H]. 1993; 207:59–66.
12. Mow VC, Ateshian GA, Spilker RL. Biomechanics of diarthrodial joints: A review of twenty years of progress. J Biomech Eng. 1993; 115:460–467. [PubMed: 8302026]
13. Linn FC. Lubrication of animal joints. I. The arthrotripsometer. J Bone Joint Surg Am. 1967; 49:1079–1098. [PubMed: 6038858]
14. Tashman S, Anderst W, Kolowich P, et al. Kinematics of the acl-deficient canine knee during gait: Serial changes over two years. J Orthop Res. 2004; 22:931–941. [PubMed: 15304262]
15. Nebelung W, Wuschech H. Thirty-five years of follow-up of anterior cruciate ligament-deficient knees in high-level athletes. Arthroscopy. 2005; 21:696–702. [PubMed: 15944625]
16. Tashman S, Anderst W. In-vivo measurement of dynamic joint motion using high speed biplane radiography and ct: Application to canine acl deficiency. J Biomech Eng. 2003; 125:238–245. [PubMed: 12751286]
17. Treece G, Prager RW, Gee AH. Regularized marching tetrahedra: Improved iso-surface extraction. Computers and Graphics. 1999; 23:583–598.
18. Anderst WJ, Tashman S. A method to estimate in vivo dynamic articular surface interaction. J Biomech. 2003; 36:1291–1299. [PubMed: 12893037]
19. Press, W.; F, B.; Teukolsky, S., et al. Numerical recipes in c: The art of scientific computing. Cambridge University Press; New York: 1998.
20. Meachim G. Light microscopy of indian ink preparations of fibrillated cartilage. Ann Rheum Dis. 1972; 31:457–464. [PubMed: 4117785]
21. Gabel R, B R. The effects of signal conditioning on the statistical analysis of gait emg. Electroenceph and Clinical Neurophysiology. 1994; 93:188–201.
22. Ristanis S, Stergiou N, Patras K, et al. Excessive tibial rotation during high-demand activities is not restored by anterior cruciate ligament reconstruction. Arthroscopy. 2005; 21:1323–1329. [PubMed: 16325082]
23. Tashman S, Kolowich P, Collon D, et al. Dynamic function of the acl-reconstructed knee during running. Clin Orthop Relat Res. 2007; 454:66–73. [PubMed: 17091011]
24. Barrance PJ, Williams GN, Snyder-Mackler L, et al. Altered knee kinematics in acl-deficient non-copers: A comparison using dynamic mri. J Orthop Res. 2006; 24:132–140. [PubMed: 16435346]
25. Defrate LE, Papannagari R, Gill TJ, et al. The 6 degrees of freedom kinematics of the knee after anterior cruciate ligament deficiency: An in vivo imaging analysis. Am J Sports Med. 2006; 34:1240–1246. [PubMed: 16636348]
26. O'Connor BL, Visco DM, Heck DA, et al. Gait alterations in dogs after transection of the anterior cruciate ligament. Arthritis Rheum. 1989; 32:1142–1147. [PubMed: 2775322]
27. Waldman SD, Bryant JT. Dynamic contact stress and rolling resistance model for total knee arthroplasties. J Biomech Eng. 1997; 119:254–260. [PubMed: 9285338]
28. Drummond C, Israelachvili J, Richetti P. Friction between two weakly adhering boundary lubricated surfaces in water. Phys Rev E Stat Nonlin Soft Matter Phys. 2003; 67:066110. [PubMed: 16241307]
29. Hills BA. Oligolamellar lubrication of joints by surface active phospholipid. J Rheumatol. 1989; 16:82–91. [PubMed: 2716011]

30. Martin JA, Brown TD, Heiner AD, et al. Chondrocyte senescence, joint loading and osteoarthritis. Clin Orthop Relat Res. 2004:S96–103. [PubMed: 15480082]
31. Wilson W, van Burken C, van Donkelaar C, et al. Causes of mechanically induced collagen damage in articular cartilage. J Orthop Res. 2006; 24:220–228. [PubMed: 16435355]
32. Wilson W, van Rietbergen B, van Donkelaar CC, et al. Pathways of load-induced cartilage damage causing cartilage degeneration in the knee after meniscectomy. J Biomech. 2003; 36:845–851. [PubMed: 12742452]
33. Rudolph KS, Snyder-Mackler L. Effect of dynamic stability on a step task in acl deficient individuals. J Electromyogr Kinesiol. 2004; 14:565–575. [PubMed: 15301775]
34. Williams GN, Snyder-Mackler L, Barrance PJ, et al. Quadriceps femoris muscle morphology and function after acl injury: A differential response in copers versus non-copers. J Biomech. 2005; 38:685–693. [PubMed: 15713288]
35. Martin JA, Buckwalter JA. Post-traumatic osteoarthritis: The role of stress induced chondrocyte damage. Biorheology. 2006; 43:517–521. [PubMed: 16912423]
36. DeFrate LE, Sun H, Gill TJ, et al. In vivo tibiofemoral contact analysis using 3d mri-based knee models. J Biomech. 2004; 37:1499–1504. [PubMed: 15336924]
37. Kiviranta I, Tammi M, Jurvelin J, et al. Topographical variation of glycosaminoglycan content and cartilage thickness in canine knee (stifle) joint cartilage. Application of the microspectrophotometric method. J Anat. 1987; 150:265–276. [PubMed: 3654339]
38. Anderst WJ, Les C, Tashman S. In vivo serial joint space measurements during dynamic loading in a canine model of osteoarthritis. Osteoarthritis Cartilage. 2005; 13:808–816. [PubMed: 15964770]
39. Herzog W, Clark A, Wu J. Resultant and local loading in models of joint disease. Arthritis Rheum. 2003; 49:239–247. [PubMed: 12687517]
40. Radin EL. Mechanical factors in the casuation of osteoarthritis. Rheumatology. 1982; 7:46–52.

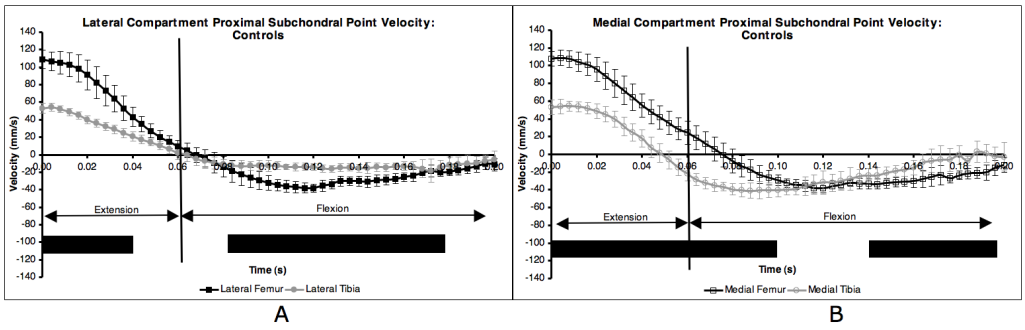

Figure 1.

Proximal subchondral point velocity in each ROI for control dogs. Averages were obtained over 10 test sessions for five dogs. Paw strike occurred at t = 0.00 s. Flexion occurred the first 60 ms after paw strike, followed by extension. Error bars are ± 1 SD. Solid line below indicates 20 ms intervals where the two curves were significantly different (KS test, $p < 0.05$).

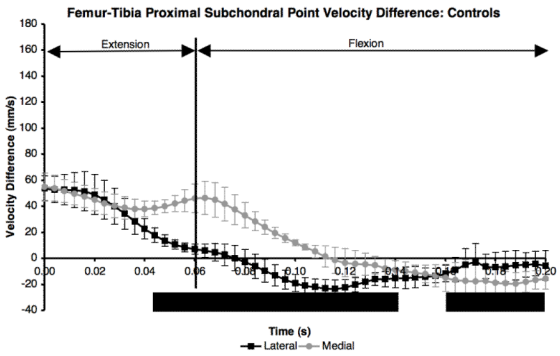

Figure 2.

Difference in proximal subchondral point velocity within each compartment for the five control dogs. Mean curves ± 1 SD for the ten test sessions were significantly different (KS test, $p < 0.05$) from 40 ms after paw strike to 140 ms after paw strike, and again from 160 ms to 200 ms after paw strike.

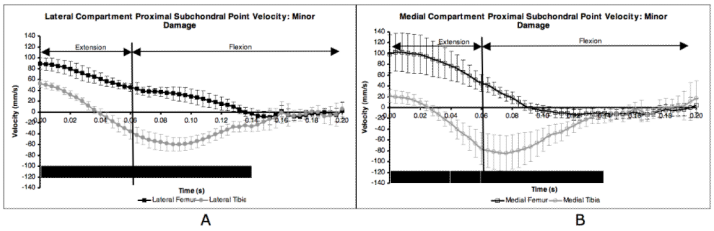

Figure 3.

Proximal subchondral point velocity in each ROI for minor damage dogs. Averages were obtained over nine post CCL-transection test sessions. Paw strike occurred at t = 0.00 s. Flexion occurred the first 60 ms after paw strike, followed by extension. Error bars are ± 1 SD and are larger than in control dog group (Figure 1) due to changes over days in CCL-deficient dogs. Solid line below indicates 20 ms intervals where the two curves were significantly different (KS test, $p < 0.05$). Major damage group curves were similar.

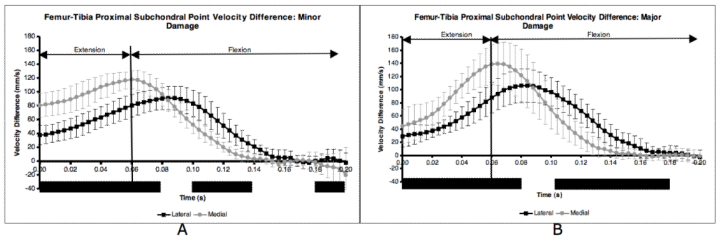

Figure 4.

Difference in proximal subchondral point velocity within each compartment for the minor damage (A) and major damage (B) dogs. Mean medial and lateral compartment curves for the nine CCL-deficient sessions were significantly different during time periods indicated by solid black bar (KS test, $p < 0.05$). Error bars are ± 1 SD.

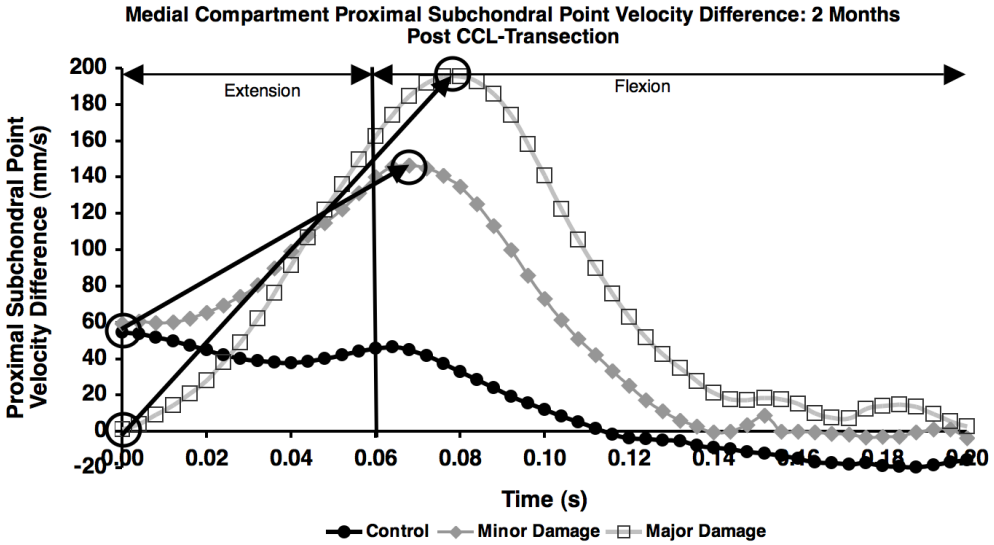

Figure 5.
Difference in proximal subchondral point velocity in the medial compartment for the control, minor damage and major damage groups on the first test session following CCL-transection. The change in proximal subchondral point velocity difference from paw strike to curve peak (noted by circles and arrows) was calculated for each test date.

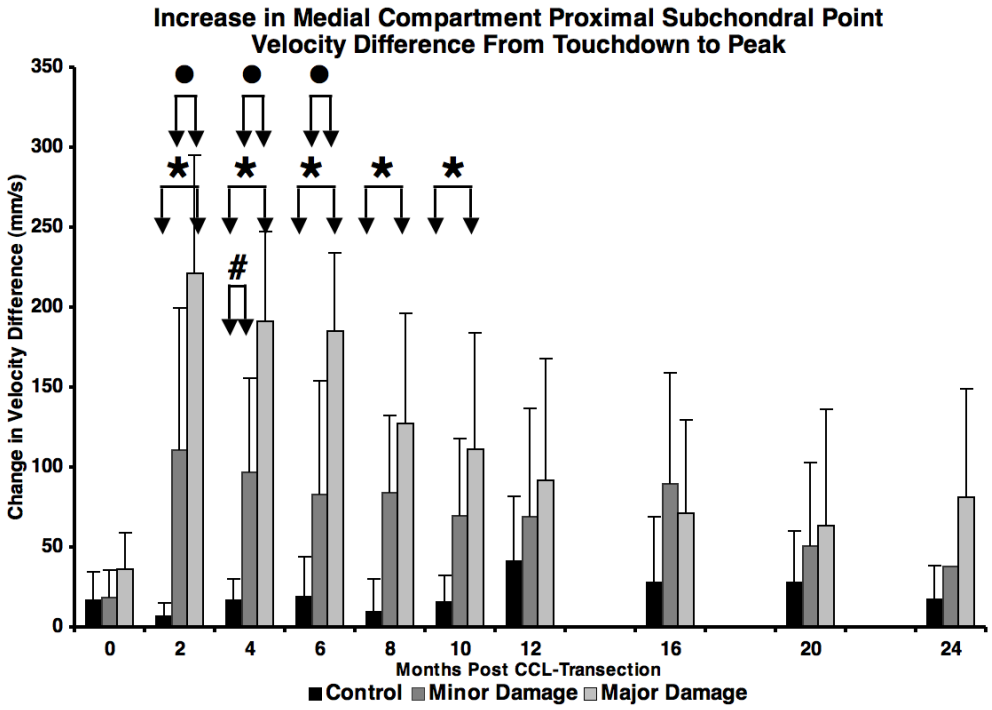

Figure 6.

Increase in medial compartment proximal subchondral point velocity difference from paw strike to velocity difference peak (arrows in Figure 5) during early stance. ● = major damage > minor damage ($p = 0.003$ to $p = 0.013$), * = major damage > control ($p < 0.001$ to $p = 0.017$), # = minor damage > control ($p = 0.036$). Error bars are one SD.

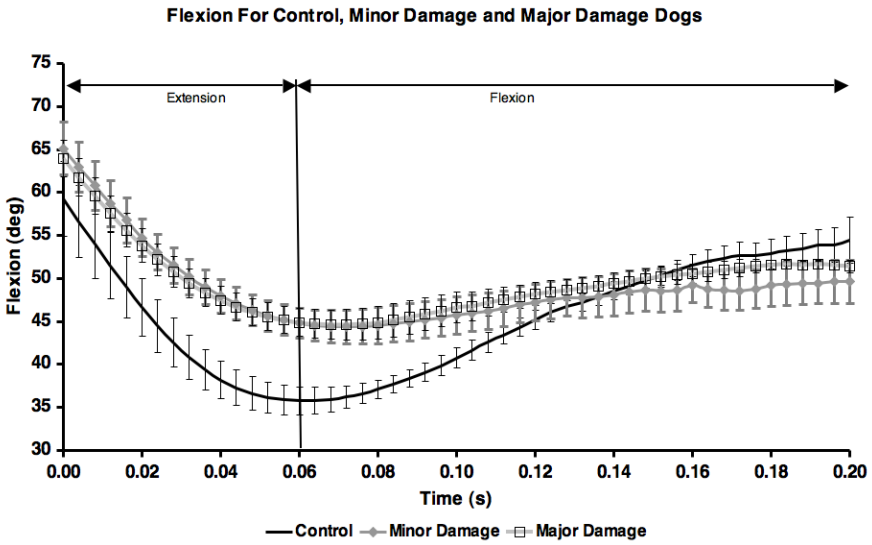

Figure 7.

Mean flexion angle for each of the three groups. Error bars are ± one standard deviation. Means for control group include all 10 test sessions. Means for minor and major damage groups are for ccl-deficient test sessions (sessions 2-10).